Available online at www.sciencedirect.com
SCIENCE DIRECT®
Journal of Sound and Vibration 280 (2005) 739–757
JOURNAL OF SOUND AND VIBRATION
www.elsevier.com/locate/yjsvi

Dynamics of ultrasonic percussive drilling of hard rocks

M. Wiercigroch[a,*], J. Wojewoda[b], A.M. Krivtsov[c]

[a]*Centre for Applied Dynamics Research, School of Engineering and Physical Sciences, King's College, University of Aberdeen, Aberdeen AB24 3UE, Scotland, UK*
[b]*Division of Dynamics, Technical University of Lodz, ul. Stefanowskiego 1/15, 90-924 Lodz, Poland*
[c]*Department of Theoretical Mechanics, St.-Petersburg State Technical University, Polytechnicheskaja 29, 195251 St.-Petersburg, Russia*

Received 6 September 2000; accepted 16 December 2003
Available online 30 September 2004

Abstract

Ultrasonic percussive drilling with diamond-coated tools has been extensively studied under laboratory conditions on rocks such as sandstone, limestone, granite and basalt, in order to investigate the applicability of this technique to downhole drilling. An experimental set-up, a programme of work and example results are presented. The studies showed that an introduction of high-frequency axial vibration significantly enhances drilling rates compared to the traditional rotary type method. It has been found out that the material removal rate (MRR) as a function of static load has at least one maximum. Looking at the time histories of the measured drilling force, strong nonlinear effects have been observed, which were explained using simple nonlinear models. Among them, pure impact and impact with dry friction oscillators were used to provide an insight into the complex dynamics of ultrasonic percussive drilling. It is postulated that the main mechanism of the MRR enhancement is associated with high amplitudes of forces generated by impacts. Novel procedures for calculating MRR are proposed, explaining an experimentally observed fall of MRR at higher static loads.

*Corresponding author. Tel.: +44-1224-272509; fax: +44-1224-272497.
E-mail address: m.wiercigroch@eng.abdn.ac.uk (M. Wiercigroch).

0022-460X/$ - see front matter © 2004 Elsevier Ltd. All rights reserved.
doi:10.1016/j.jsv.2003.12.045

1. Introduction and motivation

The harsh conditions of a downhole drilling process, its cost, and environmental issues put severe demands on the effectiveness and reliability of the drilling method. As a consequence, every increase in cutting rates and decrease in tool wear breakage is very welcome. Previous experiments carried out at the University of Aberdeen [1–3] have established the advantages of rotary high-frequency drilling for high-speed, high-precision machining of glasses, ceramics and composites. Recently, some preliminary studies have been conducted on hard rocks [3]. In particular, high material removal rates (MRRs) are achieved with substantial reduction of drilling forces when compared either with conventional grinding or conventional ultrasonic machining (USM). The approach is related to percussive drilling; however, the forcing frequency is much higher and there is a better force control. Therefore, in this paper, it is proposed to implement the already well-developed understanding of USM to downhole drilling. This work was conducted to ascertain the extent to which an introduction of high-frequency (ultrasonic) loading can improve drilling rates and reduce drilling forces, in particular, the weight on the drill bit for drilling hard rocks such as sandstone, granite and basalt [3,4].

In precision manufacturing, one of the most promising methods for drilling in hard materials is USM. In its more common form, this involves the removal of material by the abrading action of grit-loaded liquid slurry circulating between the workpiece and a tool vibrating perpendicular to the workface at a frequency above the audible range (see Fig. 1). Typically, a high-frequency power source activates a stack of magneto-strictive or piezo-electric material, which produces a

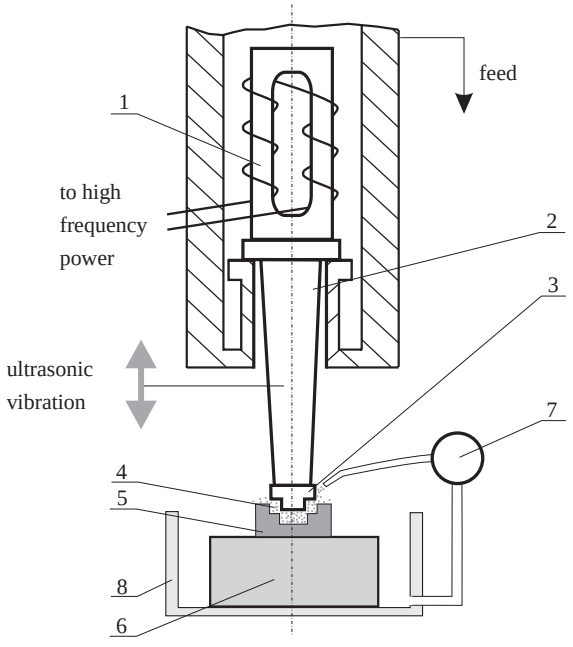

Fig. 1. Schematic of conventional USM; 1—magneto-strictive transducer, 2—coupling cone, 3—tool, 4—abrasive slurry, 5—workpiece, 6—fixture, 7 —pump, 8—tank.

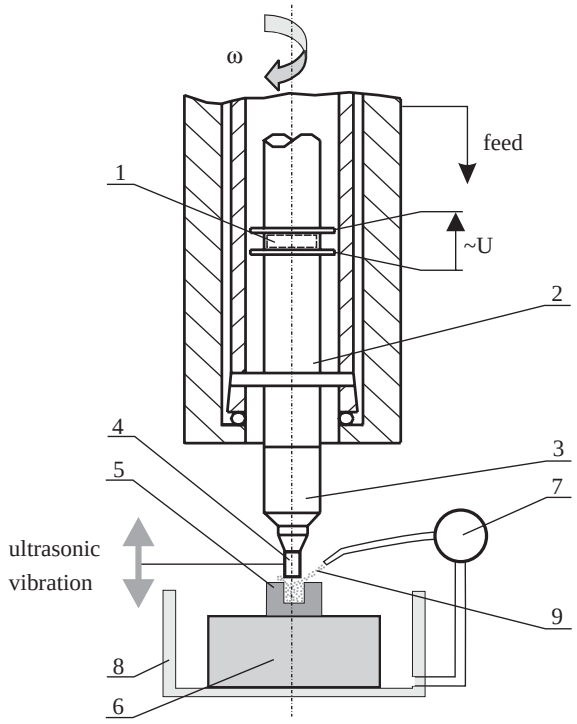

Fig. 2. Schematic of rotary USM; 1—piezo-electric element, 2—transducer assembly, 3—coupler, 4—diamond-coated or -impregnated tool, 5—workpiece, 6—fixture, 7—pump, 8—tank, 9—cutting fluid.

low-amplitude vibration of the toolholder. This motion is transmitted under light pressure to the slurry, which abrades the workpiece into a conjugate image of the tool form. A constant flow of slurry is necessary to carry away the chips from the workface. A variation of USM is the addition of ultrasonic vibration to a rotating tool, usually a diamond-plated drill (see Fig. 2). Rotary ultrasonic machining (RUM) substantially increases the drilling efficiency. A piezo-electric element (1) built into the rotating head provides the necessary vibration. The natural frequency of the transducer assembly (2) and coupler is tuned to the forcing frequency; so, ideally, the tip of a tool (4) should be at an anti-node point of the displacement. During the process, a cutting fluid (9) is supplied to cool the tool and remove debris from the workpiece (5).

As can be easily deduced, there is a strong analogy between ultrasonic drilling and downhole drilling of hard rocks, which can be used to enhance the efficiency of the downhole drilling. Therefore, the main aim of this paper is to investigate the mechanism governing the relationship between the MRRs for a selection of rocks, and various drilling parameters which can effect the process. The results from the experimental studies will form the basis for the mathematical modelling undertaken in latter sections, which is aimed to:

1. establish structurally simple but phenomenologically comprehensive models of the dynamic interactions that occurred in the ultrasonic drilling of hard rocks;

2. formulate theoretical basis to describe the ultrasonic drilling process in terms of the MRR and forces generated during the cutting action.

2. Experimental studies

2.1. Previous work

In conventional USM, abrasive grains suspended in the slurry are supplied to the gap between an ultrasonic vibrating tool and a workpiece. Under feed pressure and aided by the abrasives, the tool hammers its way into the workpiece and makes a hole. When the hole becomes deeper, ensuring a supply of abrasive to the working gap is difficult and the MRR is normally reduced. This problem was overcome by the introduction of rotary ultrasonic machining with diamond-impregnated/coated tools. These were developed in the early 1960s by UKAEA, Harwell in England. Some years later, quite similar methods were studied by Russians, e.g. Markov [5–7] and Petrukha [8], but details of the methods were not revealed. Kubota et al. [9] provided some basic concepts of the process using the experimental approach to the problem. Their experiments were carried out with three configurations; i.e. a glass plate drilled by a stationary ultrasonic tool with a rotary table, a glass rod turned by a lathe with an ultrasonic transducer on the carriage and a glass plate drilled by a rotating transducer head. They established the influences of grain size, amplitude of vibration rotational speed and feed pressure on the MRR. Similarly, Komaraiah et al. [10] conducted experiments on the USM of different workpiece materials including glass, porcelain, ferrite and alumina using various tool materials in order to analyse the effects of mechanical properties of the workpiece and tool material on the surface roughness and accuracy. In Refs. [11,12], the influence of different process parameters on the MRR during the machining of zirconia was examined. Previous studies undertaken by the authors [1] on the float glass have prompted the existence of the so-called fall in MRR for higher rates of static load. These works confirmed once again the superiority of the rotary technique over conventional slurry-type drilling.

2.2. Experimental rig and programme

The experimental studies have been conducted on a rotary ultrasonic milling machine developed at the University of Aberdeen and known as the ‘Ultramill’ [13]. This machine is design-based on a commercial jig-borer with vertical roller slideways carrying the ultrasonic head assembly. The headstock consists of a piezo-electric ultrasonic transducer operating at 21 kHz and rotating on two ball bearings mounted at ultrasonic displacement node points, the spindle being directly driven by a DC motor. Tools are mounted by means of a screw thread, with a plane interface positioned close to a stress node, to provide the ultrasound coupling. There are two different types of diamond tools, diamond impregnated and diamond coated. With impregnated tools, the diamond grids are bonded into the parent material of the tool, where with coated tools a thin layer of diamonds is bonded by electroplating to a blank tool made from mild steel. During the course of the experimental studies, only the diamond-coated tools were used.

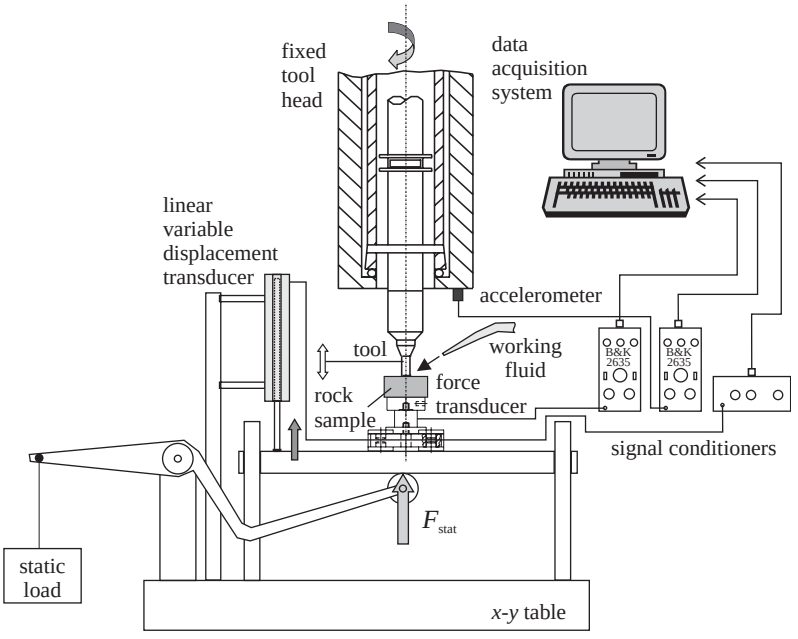

Fig. 3. Schematic of the experimental rig.

A unique programme of experimental investigations was carried out to determine the relationships between the MRR and the process control parameters including the static load, ultrasonic amplitude, and rotational speed of the spindle. In order to ascertain these relationships, an experimental rig shown in Fig. 3 was used, which comprises of the Ultramill, a load cell, and displacement and acceleration transducers.

In a typical test, the following signals were recorded: the acceleration of the headstock measured by an accelerometer, the dynamic drilling force by a force transducer, the vertical displacement by a Linear Variable Displacement Transducer (LVDT). A drilled sample waxed to the micro-table of the load cell was clamped to the cross table of the ultrasonic drilling machine. During the drilling process, the transducer signals were connected to the input channels of the data acquisition system, which acquired data with a sampling rate of up to 800 kHz. The experimental data were then analysed off-line by playing back the digital records.

A schematic of the experimental rig depicted in Fig. 3 also shows a mechanism of applying constant static force, F_{stat}. The mechanism uses gravity of required weights to move the sample towards the tool. Throughout the experimental studies the headstock position remained fixed, and the rock samples were lifted and pressed against the tool. At the beginning of each test, the static load was gently applied to the rock sample through the load release system lever until it reached the required value. During the drilling process the working fluid was supplied to remove the debris and cool the drill.

The programme of experimental studies included 758 drilling tests on four different stones such as sandstone (three different types), limestone (one type), granite (one type), basalt (five types) and on a float glass. The experiments on the float glass were to relate the current findings with the previous studies (e.g. Ref. [1]). For each test the following parameters were chosen: drilled

material static load, ultrasonic amplitude, rotational speed, tool diameter and diamond grid size. Then, for each test, a unique data file has been produced and stored for further analysis and calculation of the MRRs. Since the majority of our tests comply with the same pattern, only sample results are discussed here. In particular, results obtained for the Hopeman sandstone will be discussed in the next section.

2.3. Experimental results

Almost all previous experimental results and most theoretical approaches (e.g. Ref. [14]) have concentrated on the static relationships between MRR and F_{stat}, which can hardly explain the role of vibrations in the ultrasonic drilling. It has been recently repeatedly observed in our laboratory that the main working mechanism is related to impact oscillators [1,2,15,16].

Figs. 4 and 5 show steady-state time histories of the drilling force for four different levels of the static load and the ultrasonic amplitude. These time histories suggest that the considered process is nonlinear due to the fact that the tool impacts the workpiece. The closest model for this action is an impact oscillator with a gap, which can be altered to control the amplitude of the generated percussive forces. On top of this, additional effects such as modulations are also visible.

The strong modulation of the signal amplitude clearly visible on the condensed time histories of Figs. 4 and 5 is caused by rotation of the spindle. There are also weak modulations seen on the zoom-up plots; however, no convincing explanation can be given yet. By examining Fig. 4 (both the condensed and the zoom-up time histories), it is evident that the static load of 25 N produces the highest impact forces, leading consequently to a higher value of the MRR. This finding coincides with the theoretical predictions, for both the single-degree-of-freedom (dof) and three-dof models, which will be given in the next sections. It is also noticeable that the system vibrates with period two motion for all the four static loads.

Some qualitative motion changes are apparent when the ultrasonic amplitude is being used as a control parameter (see Fig. 5). It starts with nearly a period one motion of a small amplitude at $a_{um} = 3.5\,\mu\text{m}$, develops a period two motion with a slightly larger amplitude at $a_{um} = 4.5\,\mu\text{m}$, to settle on a period two with a large amplitude of the measured force oscillations for $a_{um} = 5.5$ and $7.0\,\mu\text{m}$. The influence of the static load and the ultrasonic amplitude on the measured force is strongly nonlinear, so even a small difference in amplitude (Fig. 5(b) and (c)) can produce a change in dynamic response. This can clearly be seen on zoom-ups of the above-specified time histories (Fig. 5(f) and (g)), where the tip of the tool after an impact with the workpiece spends a half of the period oscillating with significantly smaller amplitude (Fig. 5 (g)).

Examining the changes in the dynamic responses depicted in Fig. 5(a) and (b), one can notice the behaviour similar to those reported for other impacting systems, e.g. Refs. [17,18]. A high-amplitude period two motion leads consequently to the saturation of the MRR, and this is predicted theoretically in the next section.

Although the dynamic responses are interesting and possibly carrying the answers on the working mechanism, the most important practical information is the MRR. Fig. 6 presents the MRR obtained by varying the static load and ultrasonic amplitude. The tool progression time histories depicted in Fig. 6(a) and (b) reveal complexities of the drilling process, such as the percussive action, propagating fracture, and stochasticity of the rock mechanical properties. This is reflected in irregularities of time histories of the tool progression. However, it is clear that the

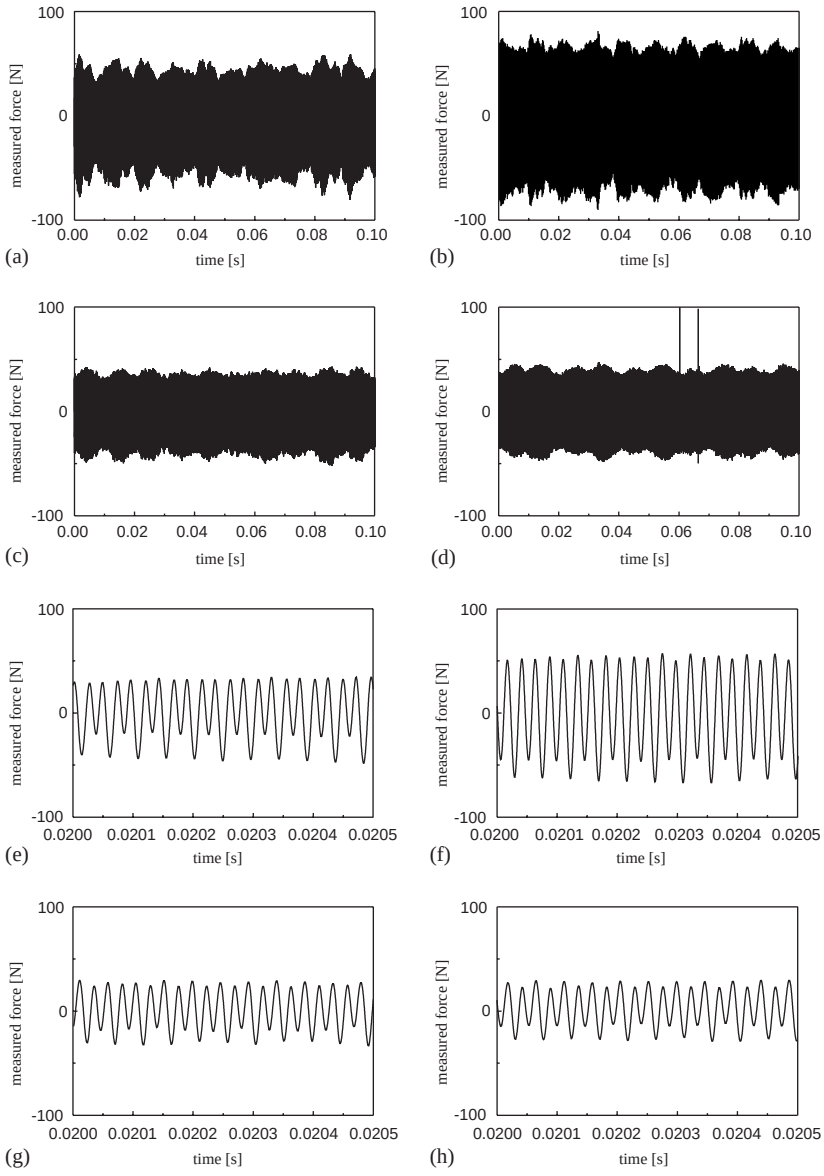

Fig. 4. Time histories of the percussive force for a varying load and constant ultrasonic amplitude, $a_{um} = 5\,\mu m$; time span within 0.1 s: (a) $F_{stat} = 20\,N$, (b) $F_{stat} = 25\,N$, (c) $F_{stat} = 30\,N$, (d) $F_{stat} = 35\,N$, (e)–(h) zoom-ups of (a)–(d) within the time span of 0.0005 s.

average tool progression as a function of ultrasonic amplitude increases monotonically (see Fig. 6(a) and (c)) to reach the saturation zone, which is best observed on the MRR (Fig. 6(c)).

The fall of the MRR for higher static loads can be easily seen by examining Fig. 6(b) and (d). Also, an existence of multiple maxima for different ultrasonic amplitudes was observed.

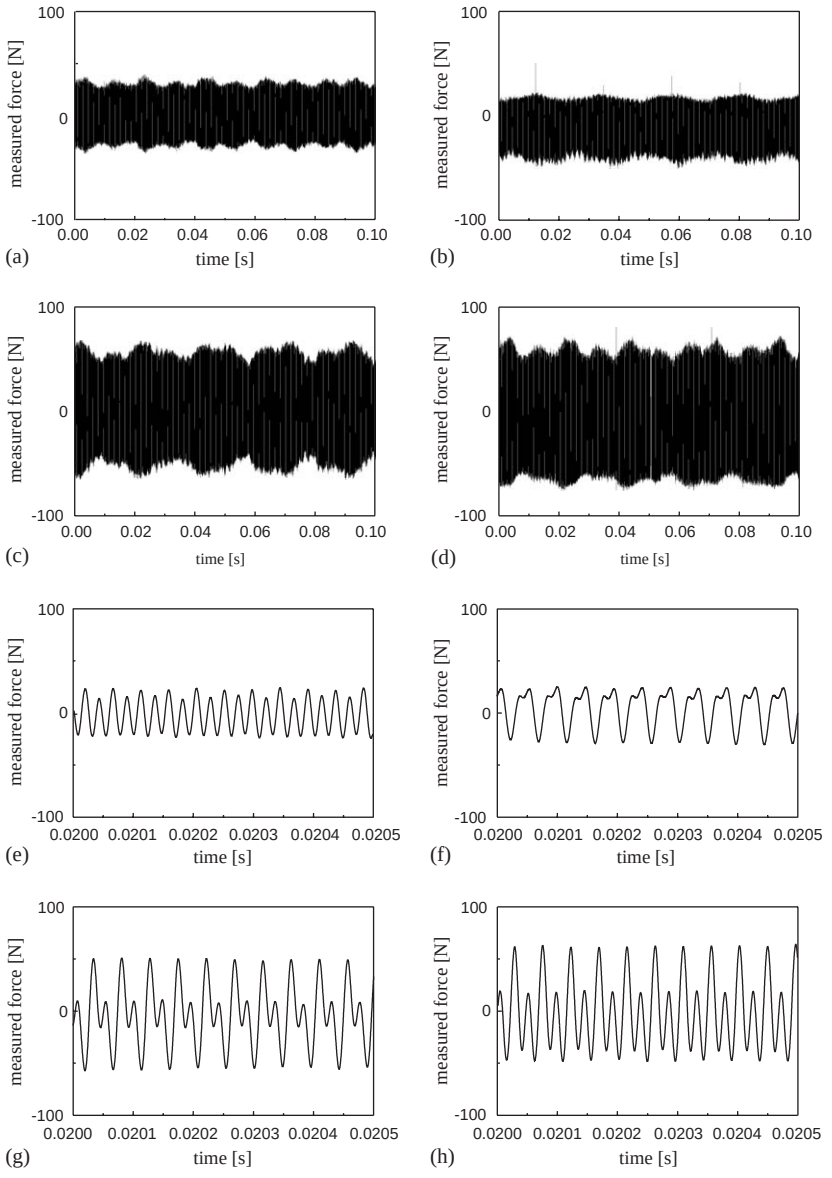

Fig. 5. Time histories of the percussive force for a varying ultrasonic amplitude and constant load $F_{\text{stat}} = 25\,\text{N}$; time span within 0.1 s: (a) $a_{um} = 3.5\,\mu\text{m}$, (b) $a_{um} = 4.5\,\mu\text{m}$, (c) $a_{um} = 5.5\,\mu\text{m}$, (d) $a_{um} = 7\,\mu\text{m}$, (e)–(h) zoom-ups of (a)–(d) within the time span of 0.0005 s. The zoom-ups have been taken in the sections of the lowest amplitudes.

Summarizing, the introduction of the high-frequency axial percussive motion substantially increases the MRR, while compared to the conventional drilling (without axial vibrations). For the data presented in this study, the enhancement is approximately ten times. It is noteworthy to point out that the largest value of F_{stat} does not produce the largest impacts.

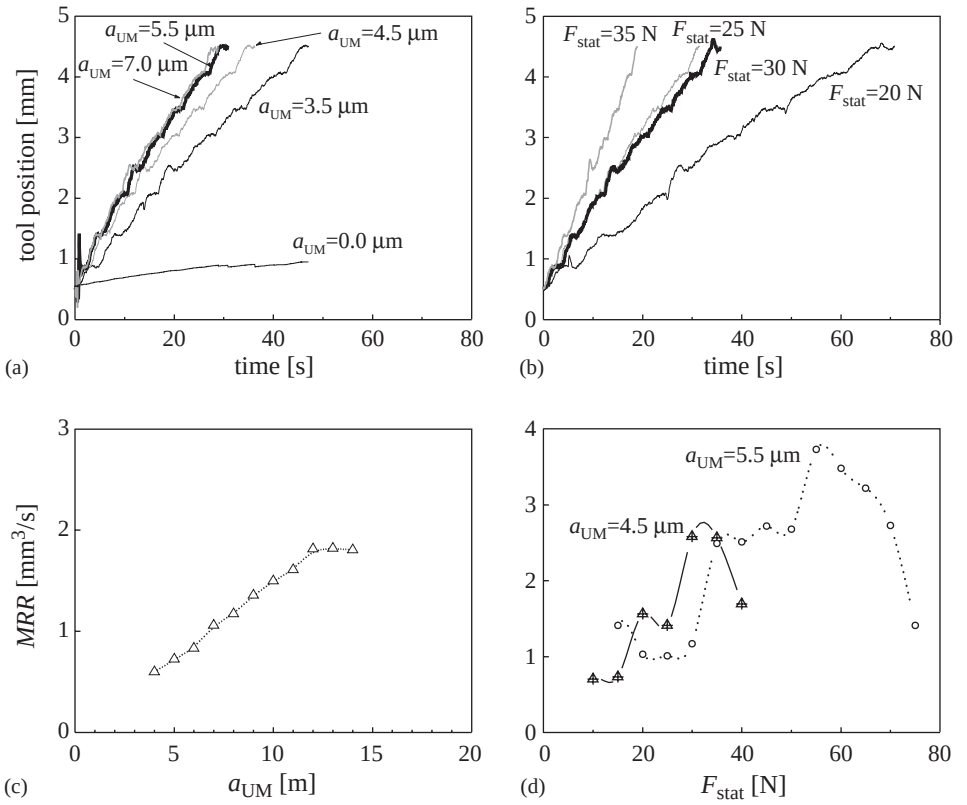

Fig. 6. Tool progression and the MRR for the Hopeman sandstone: (a) tool progression for constant static load of 70 N and varying ultrasonic amplitude, (b) tool progression for constant ultrasonic amplitude of 5.5 μm and varying static load, (c) MRR for the case (a), and (d) MRR for the case (b).

3. Theoretical modelling

The first theoretical approach to modelling of USM was put forward by Saha et al. [14]. This attempt was to develop a comprehensive analytical model for the estimation of MRR in order to investigate the mechanism of the material removal process. The paper reports a satisfactory agreement between theory and experiment, apparently explaining the fall in MRR for higher static loads. However, this model uses Hertzian theory to explain the mechanism of material removal. It appears that this should be more suitable for ductile rather than brittle materials. A theoretical model based on indentation fracture mechanics was presented in Ref. [12]. The model gives a reasonable correlation with the experimental data, but it cannot predict MRR before commencing experimental studies since the calculation requires the power-rating evaluation, which has to be taken from the experimental data. Another empirical model was proposed in Ref. [11], where the machining process is carefully monitored and analysed. Based on a number of experiments of carefully chosen parameters, the model can be used in MRR prediction over a wider range of process parameters. However, this model is static and therefore it is not capable of explaining the dynamics of ultrasonic drilling.

3.1. Three-dof model without progression

Dynamics for ultrasonic drilling with a resonant transducer assembly tuned to the ultrasonic frequency can be modelled as a two-mass discrete model, which was analysed in Ref. [2]. For the purpose of clarity, this paper summarizes the main results.

The model shown in Fig. 7 consists of a mass representing the movable headstock, m_1, and the equivalent mass of the vibrating ultrasonic horn plus tool, m_2. Linear springs of stiffness k_1 and k_2 and dashpots of viscous damping c_1 and c_2 connect the head-stock and the equivalent mass to the piezo-electric ultrasonic driver, which excites the system kinematically with amplitude A and frequency $\Omega/(2\pi)$. The material properties are represented by a stiffness k_3 and damper c_3. The process starts with an initial gap g between the tool tip and the workpiece. The model assumes that the influence on the dynamic responses coming from penetration into the material can been

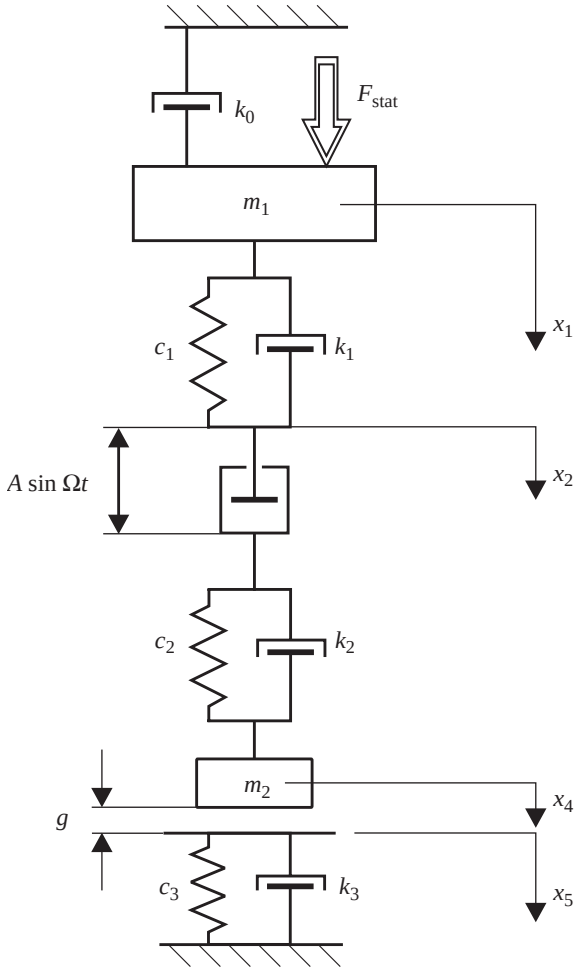

Fig. 7. Three-dof model of ultrasonic drilling.

neglected. The equations of motion for the system are piecewise linear of the following form:

$$m_1\ddot{x}_1 + c_0\dot{x}_1 + c_1(\dot{x}_1 - \dot{x}_2) + k_1(x_1 - x_2) = F_{\text{stat}}, \tag{1}$$

$$c_1(\dot{x}_2 - \dot{x}_1) + c_2(\dot{x}_2 - A\Omega\cos\Omega t - \dot{x}_4) + k_1(x_2 - x_1) + k_2(x_2 - A\sin\Omega t - x_4) = 0, \tag{2}$$

$$m_2\ddot{x}_4 + c_2(\dot{x}_4 - \dot{x}_2 + A\Omega\cos\Omega t) + k_2(x_4 + A\sin\Omega t - x_2) = 0 \quad \text{for } x_4 - x_5 \leqslant g \text{ and } \dot{x}_4 < \dot{x}_5, \tag{3}$$

$$m_2\ddot{x}_4 + c_2(\dot{x}_4 - \dot{x}_2 + A\Omega\cos\Omega t) + c_3\dot{x}_5 + k_2(x_4 + A\sin\Omega t - x_2) + k_3x_5 = 0 \quad \text{for } x_4 - x_5 > g \text{ and } \dot{x}_4 \geqslant \dot{x}_5, \tag{4}$$

$$c_3\dot{x}_5 + k_3x_5 = 0 \quad \text{for } x_4 - x_5 \leqslant g \text{ and } \dot{x}_4 < \dot{x}_5, \tag{5}$$

$$\dot{x}_5 = \dot{x}_4 \quad \text{for } x_4 - x_5 > g. \tag{6}$$

It was assumed that the MRR is a function of the magnitude of the impact force and its frequency [19–22] and the tip of the tool, with diamonds uniformly distributed, impacts the workpiece making micro-cracks on its surface. The relative value of MRR was estimated from the algorithm developed in Ref. [2], which is briefly outlined below:

1. Initially, the global average value AVG* of the impact force (see Eq. (8) and Fig. 8), IF, over all numerical simulations performed is calculated from

$$\text{AVG}^* = \frac{1}{m}\sum_{i=1}^{m}\frac{1}{t_2 - t_1}\int_{t_1}^{t_2}\text{IF}(t)\,\mathrm{d}t, \tag{7}$$

where m is the number of numerical simulations, t_1, t_2 are the time limits of a single simulation chosen to provide a steady-state time history. Eq. (7) can be re-written for a discrete time

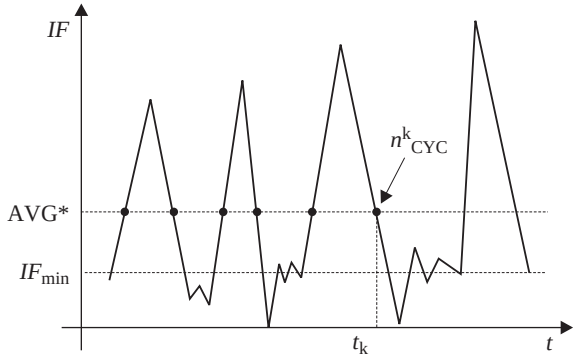

Fig. 8. Diagram used for calculating MRR, where AVR* is the globally average impact force, $\text{IF}_{\min}$ is the minimum impact force causing a crack, n^k_{CYC} and t_k is the number and the time of kth crossing of AVR*.

series as

$$\mathrm{AVG}^* = \frac{1}{m}\sum_{i=1}^{m}\frac{1}{n}\sum_{j=1}^{n}\mathrm{IF}_{ij}, \tag{8}$$

where IF_{ij} is an impact force calculated for the jth time step of the ith simulation.

2. The minimum impact force $\mathrm{IF}_{\min}$ causing damage is assumed to be dependent on the material constant

$$\mathrm{IF}_{\min} = a\,\mathrm{AVG}^*. \tag{9}$$

3. The effective crack propagation force IF^* is assumed to be

$$\mathrm{IF}^* = \mathrm{IF} - \mathrm{IF}_{\min} \quad \text{for } \mathrm{IF} > \mathrm{IF}_{\min}, \tag{10}$$

$$\mathrm{IF}^* = 0 \quad \text{for } \mathrm{IF} \leqslant \mathrm{IF}_{\min}. \tag{11}$$

4. Similar to the calculation of fatigue life, it is postulated that MRR will be dependent on the number of cycles, which is evaluated from a number of times the AVG^* line is crossed

$$n_{\mathrm{cyc}} = n_{\mathrm{cross}}/2. \tag{12}$$

5. Finally, the MRR is then estimated as

$$\mathrm{MRR} = \frac{n_{\mathrm{cyc}}}{(t_1 - t_2)}\frac{1}{n}\sum_{i=1}^{n}\left(\frac{\mathrm{IF}_i^*}{\mathrm{AVG}^*}\right)^z \mathrm{IF}_i, \tag{13}$$

where n is the number of time steps and z is currently a free parameter chosen from comparison with experimental results.

An example of MRR calculated using the above algorithm for varying static load is shown in Fig. 9, which has been normalized with respect to the maximum values of F_{stat} and MRR. From a careful examination of the graph, it is evident that the upper and lower envelopes are non-monotonic functions of F_{stat} with well-pronounced maxima. The jagged edge of the MRR graph is due to the nonlinear dynamic responses of the system, which are studied in the section to follow.

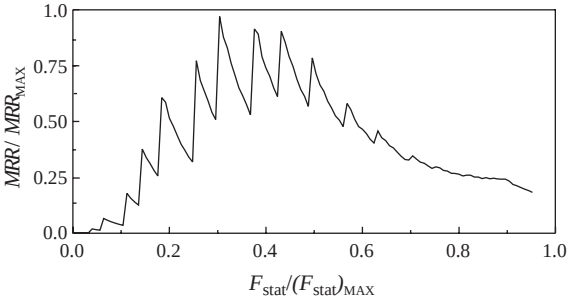

Fig. 9. The MRR as a function of F_{stat}.

However, it is worth noting that the envelopes correlate well with the experimental findings, particularly in predicting the experimentally observed drops in MRR (see Fig. 6(d)).

The main role of F_{stat} is to provide conditions for the most effective impacting patterns. Clearly, under certain conditions, the light load causes the head to 'bounce off' the workpiece, with only intermittent and small impact forces. However, when F_{stat} is too large, the hammering effect disappears and the workpiece is loaded with a force that possesses a large static component, decreasing significantly the cutting efficiency.

3.2. One-dof model with progression

The current section will investigate the nonlinear dynamics approach to model the MRR, which is phenomenologically different from any others previously undertaken, including the 3-dof model outlined in the previous section. It is based on the theory of impacting and dry friction oscillators [15–18]. In particular, the formulation of a simple model of the nonlinear dynamic interactions encountered during the drilling process will be addressed, which aims to explain the fall in the MRR for higher static loads and also take into account a progressive motion of the drilling tool.

The presented model is shown in Fig. 10, where m is an equivalent mass of the tool, $F(t)$ is a drilling force, $P(\dot{y})$ is a resistive force modelled by a frictional pair, x is coordinate of the tool's tip, and y is coordinate of the dry friction element, which represents progression of the drilling surface. The equation of motion of the mass takes the following form:

$$\begin{aligned} m\ddot{x} &= F(t) \quad \text{for } x < y, \\ m\ddot{x} &= F(t) - P(\dot{y}) \quad \text{for } x = y, \end{aligned} \tag{14}$$

which depends on the relative position between x and y coordinates. The equation of motion for the frictional slider is

$$\begin{aligned} y &= x \quad \text{for } \dot{x} \geqslant 0, \\ \dot{y} &= 0 \quad \text{for } \dot{x} < 0. \end{aligned} \tag{15}$$

In reality, the drilling force has static and dynamic components. It was assumed the drilling force $F(t)$ has the following form:

$$F(t) = F_{stat} + F_{dyn} \sin(\omega t + \phi_0), \tag{16}$$

where F_{stat} is the static force, F_{dyn} and ω are the amplitude and frequency of harmonic force, relatively, t is time, and ϕ_0 is a phase shift. The resistive force $P(\dot{y})$, which in reality is very

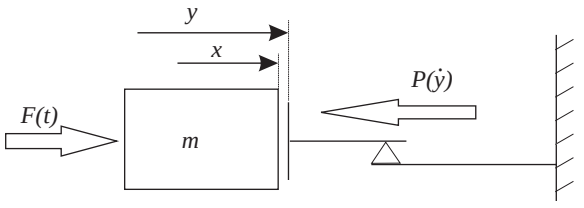

Fig. 10. One-dof model with a dry friction pair.

complex, is modelled by a Coulomb friction in the first instance. This requires a fulfillment of the following conditions:

$$P(\dot{y}) = Q \quad \text{for } \dot{y} > 0,$$

$$P(\dot{y}) \leqslant Q \quad \text{for } \dot{y} = 0, \tag{17}$$

where Q stands for modulus of the dry friction force. Consideration will be limited to the case when $F(t) < Q$. From Eqs. (14)–(17), it can be easily seen that the considered system can be in one of three unique modes listed in Table 1.

In order to gain some extra flexibility, new dimensionless variables and parameters are introduced:

$$\tau = \omega t, \quad f(\tau) = \frac{F(t)}{Q}, \quad a = \frac{F_{\text{dyn}}}{Q}; \quad b = \frac{F_{\text{stat}}}{Q}, \quad \xi = \frac{\omega^2 m}{Q}\, x, \quad \eta = \frac{\omega^2 m}{Q}\, y. \tag{18}$$

The dimensionless drilling force takes the form

$$f(\tau) = a \sin(\tau - \omega t_0) + b < 1\,. \tag{19}$$

Numerical analysis of the system shows that when the static force is large enough only periodic motion with the excitation frequency occurs. For b/a above the first subcritical period of doubling bifurcation located at $b/a \approx 0.27$, the system responds with a period one motion, as shown in Fig. 11. All bifurcation diagrams presented here were obtained for $a/Q = 0.12$ and for the static force, b varying from zero up to the value of the dynamic component, a.

Fig. 11 shows that, after the second subcritical period doubling, a narrow region of chaotic motion occurs, followed by period three and then period six motions. Then again a narrow chaotic region is seen, which is followed by period four and period eight motions. Thus, after each chaotic region, multiplicity of the motion increases by one period. It is clear from Fig. 11 that for this system chaotic regions are quite narrow whilst compared to periodic ones. A similar behaviour has been reported for two-dimensional piecewise smooth maps, e.g. Refs. [23,24].

From the practical point of view, the drilling progression per excitation period, $\Delta\eta$ is an important measure. This progression normalized to the maximum value of 1 as a function of the drilling forces ratio is presented in Fig. 12 as a function of the drilling force ratio, b/a.

From Fig. 12, one can deduce that the maximum value of the progression is obtained for the period one motion. For the responses with multiple periods, high progressions occur at certain values of the drilling forces ratio, but it is necessary to note that the responses need to be averaged; hence the material removal became smaller than for the period one motion, as

Table 1
Three unique modes of motion

Mode	x	y	Condition
No contact	$m\ddot{x} = F(t)$	$\dot{y} = 0$	$x < y$
Progression	$m\ddot{x} = F(t) - Q$	$y = x$	$\dot{x} > 0$
Stop	$\dot{x} = 0$	$y = x$	$F(t) \geqslant 0$

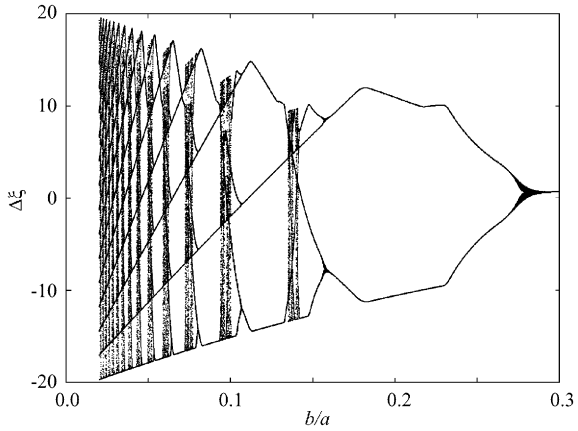

Fig. 11. Bifurcation diagram of tool displacement per excitation period $\Delta\xi$, as a function of the drilling forces ratio b/a.

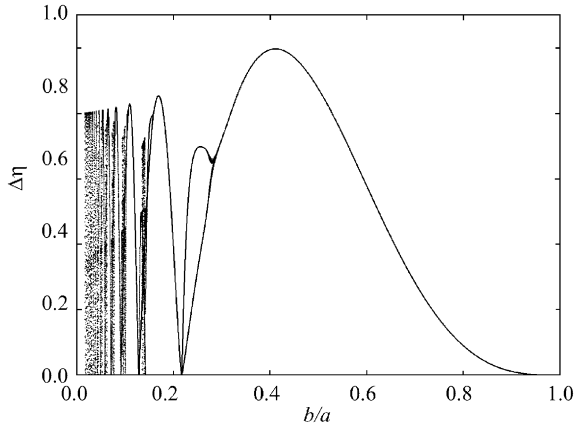

Fig. 12. Bifurcation diagram of the drilling surface displacement $\Delta\eta$ per excitation period, as a function of the drilling forces ratio b/a.

shown in Fig. 13. In this figure, the MRR is shown as a function of the drilling forces ratio, b/a. The MRR is assumed to be proportional to the average progression of the drilling surface and is shown with respect to its maximum value. An interesting and rather unexpected result is that for certain values of the drilling forces ratio the MRR decreases to zero. The local maxima of the MRR which are related to subharmonics, and therefore some impacts, are strong, and others are weak. Consequently, this might result in a low MRR and possibly in a high tool wear.

Now a progressive periodic motion is investigated, as shown in Fig. 14, which satisfies the following equations:

$$\xi(\tau + 2\pi) = \xi_* + \xi(\tau), \quad \eta(\tau + 2\pi) = \xi_* + \eta(\tau), \tag{20}$$

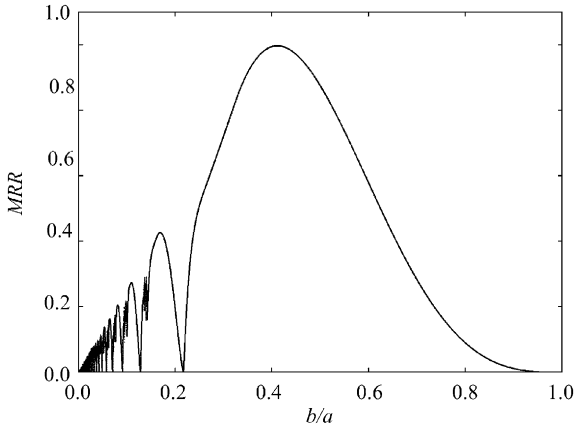

Fig. 13. MRR as a function of the drilling forces ratio b/a.

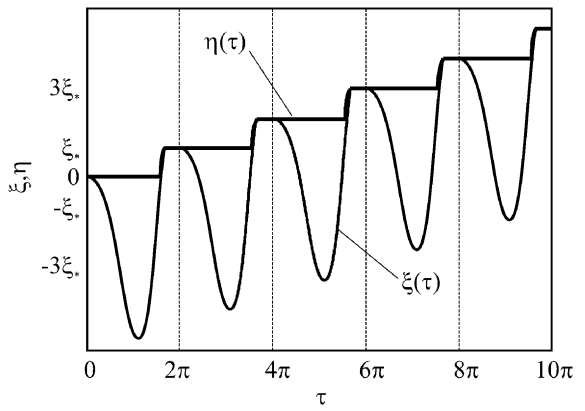

Fig. 14. Progressive periodic motion.

where ξ_* is the dimensionless penetration during one excitation period. The dimensionless MRR calculated per one period is

$$r = \frac{\eta(2\pi - \eta(0)}{2\pi} = \frac{\xi_*}{2\pi}. \tag{21}$$

Substitution of the stationary solution to the equation of motion leads to a set of algebraic nonlinear equations, which will be discussed below.

MRR as functions of the force ratios b/a ($a = \text{const}$) and b/a ($b = \text{const}$) are shown in Fig. 15. The thick curves in both figures are calculated for a soft excitation, i.e. $a \to 0$ or $b \to 0$. In the left-hand side figure, the curves above the thick one correspond to $a = 0.1, 0.2, \ldots, 0.5$, while in the right-hand side figure the curves correspond to $b = 0.05, 0.10, \ldots, 0.25$.

In Fig. 15(a), the relationships between the MRR and the static force b have clearly pronounced maxima and for the ratio b/a equal to one the MRR decreases to zero. The curves above the thick

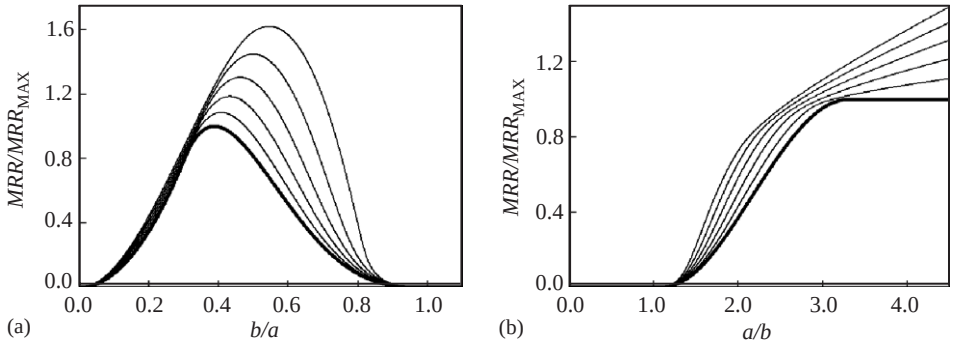

Fig. 15. MRR as functions of (a) the relative hydrostatic force b/a ($a = \text{const}$), and (b) the relative amplitude of the harmonic force a/b ($b = \text{const}$).

one correspond to hard excitations, calculated using small-parameter approximation [15]. It can be deduced from the graphs that the MRRs for hard excitations also have well-pronounced maxima, but they are shifted to higher values of b/a.

Consider now the influence of the amplitude of the harmonic force a on the MRR while the static force b is kept constant, as shown in Fig. 15(b). The MRR is equal to zero for $a \leqslant b$, then it increases monotonically to finally reach a constant value for $a/b > \sqrt{1+\pi^2}$. Hence, there is no need to increase amplitude of the harmonic force above $3.3b$. The curves above the thick one in Fig. 15(b) correspond to hard excitation. The vertical axes are presented as ratios to $\text{MRR}_{\max}$, which is calculated using small-parameter approximation [15] and can be expressed as

$$\text{MRR}_{\max} = \pi \frac{QSb^2}{\omega m}, \tag{22}$$

where S is the cross-section of the drillbit. For the hard excitation, the MRR is a monotonic function of the excitation amplitude, b. It is noteworthy that, for a bigger excitation, the MRR does not have the flat portion, and the inclination of this part of the graph is steeper for higher values of b.

The developed model allows the calculation of the MRR in the form

$$\text{MRR} = \frac{SQ}{\omega m} r(a,b), \tag{23}$$

where $r = r(a,b)$ is a known function of a and b.

An investigation of the MRR function given by Eq. (22) provides the following conclusions:

1. Impacting action is only effective if the static force is smaller than the amplitude of the harmonic force, $b < a$. If b is greater than a, the drill is stopped by the static force.
2. For the lower static forces (approximately $b < 0.3a$), motion with the period of the excitation force became unstable and multi-period or chaotic motion occurs, which is characterized by a smaller MRR and higher wear of the tool.
3. The MRR function of the static force, B (while A is kept constant), has a well-pronounced maximum, which is taken at $b \approx 0.39a$ for soft excitation and shifts to the right for greater excitation.

4. The MRR is a monotonically increasing function of the amplitude of the harmonic force, a. In the case of the soft excitation, this function becomes constant for $a/b > \sqrt{1+\pi^2}$; this means that an increase of the amplitude more than $3.3b$ does not improve the MRR.

4. Conclusions

The conducted experimental studies on a variety of different rocks have concluded that the introduction of the high-frequency oscillatory motion significantly increases their MRRs. By examining the influence of the static loading it has been found out that the MRR has at least one maximum. The MRR as a function of the ultrasonic amplitude saturates for higher values of the amplitudes. Time histories of the dynamic drilling force indicate strong nonlinear effects associated mainly with the impacting action of the tool. However, other effects such as propagating fracture and stochasticity of rock mechanical properties are also important factors, and will be addressed in the ongoing research [22].

A theoretical study has also been carried out to investigate the mechanism governing the high-frequency (ultrasonic) percussive (impact) drilling of hard brittle materials such as rocks. First, a three-degrees-of-freedom model was studied using an impact oscillator approach. This was the first dynamic model able to explain the fall of the MRR for higher static forces. It was also noted that a light static load causes the tool to be 'bounced off' from the workpiece, with only intermittent and small impact forces. On the contrary, when the static force is too large, the percussive effect disappears and the workpiece is exposed to a static force decreasing drastically the drilling efficiency. When the ultrasonic amplitude was varied, the MRR initially increased to reach a saturation value for higher static loads. The predicted nonlinear character of its behaviour was investigated by a single-degree-of-freedom model, where a comprehensive nonlinear dynamic analysis including construction of MRR bifurcation diagrams was conducted. Moreover, the most intriguing phenomenon of zero MRR for some discrete values of the static load has been observed. The developed analytical expressions describing the MRR confirmed the existence of maxima for moderate values of the static load.

Acknowledgements

The authors would like to thank anonymous reviewers for their constructive comments. The financial support from the Royal Society of London, the Centre for Marine and Petroleum Technology and the Engineering and Physical Sciences Research Council is gratefully acknowledged.

References

[1] M. Wiercigroch, R.D. Neilson, M.A. Player, H. Barber, Experimental study of rotary ultrasonic machining: dynamic aspects, *Machine Vibration* 2 (1993) 187–197.

[2] M. Wiercigroch, R.D. Neilson, M.A. Player, Material removal rate prediction for ultrasonic drilling of hard materials using an impact oscillator approach, *Physics Letters A* 259 (1999) 91–96.
[3] M. Wiercigroch, A. Krivtsov, J. Wojewoda, Dynamics of high frequency percussive drilling of hard materials, in: M. Wiercigroch, B.D. Kraker (Eds.), *Nonlinear Dynamics and Chaos of Mechanical Systems with Discontinuities*, World Scientific, Singapore, 2000, pp. 403–444.
[4] M. Wiercigroch, P.W. Glover, Confidential Final Report on Enhanced Resonance Drilling, Project No. RGD 0528, Centre for Marine and Petroleum Technology, London, 2001.
[5] A.I. Markov, I.D. Ustinov, A study of the ultrasonic diamond drilling of non-metallic materials, *Industrial Diamond Review* 3 (1972) 97.
[6] A.I. Markov, Ultrasonic drilling and boring of hard non-metallic materials with diamond tools, *Stanki i Instrument* 48 (1977) 33 (in Russian).
[7] A.I. Markov, *Ultrasonic Machining of Materials*, Mashinostroenie, Moscow, 1980 (in Russian).
[8] P.G. Petrukha, Ultrasonic diamond drilling of deep holes in brittle materials, *Russian Engineering Journal* L10 (1980) 70–75.
[9] M. Kubota, J. Tamura, N. Shimamura, Ultrasonic machining with diamond impregnated tools, *Precision Engineering* 11 (1977) 127.
[10] M. Komaraiah, M.P. Mannan, P.N. Reddy-Narasimha, S. Victor, Investigation of surface roughness and accuracy of ultrasonic machining, *Precision Engineering* 10 (1988) 58.
[11] Z.J. Pei, D. Prabhakar, P.M. Ferreira, M. Haselkorn, A mechanistic approach to the prediction of material removal rates in rotary ultrasonic machining, *Journal of Engineering for Industry* 117 (1995) 142–151.
[12] D. Prabhakar, P.M. Ferreira, M. Haselkorn, An experimental investigation of material removal rates in rotary ultrasonic machining, *Transactions of the North American Manufacturing Research Institution of SME* 99 (1992) 211–218.
[13] H. Barber, M.A. Player, Ultrasonic Milling Machine, Report of the Department of Physics, University of Aberdeen, 1987.
[14] J. Saha, A. Bhattacharyya, P.K. Mishra, Estimation of material removal rate in USM process: a theoretical and experimental study, *Proceedings of the 27th MATADOR Conference*, UMIST, Manchester, April 1988, pp. 275–279.
[15] A. Krivtsov, M. Wiercigroch, Dry friction model of percussive drilling, *Meccanica* 34 (6) (1999) 425–435.
[16] A. Krivtsov, M. Wiercigroch, Penetration rate prediction for percussive drilling via dry friction model, *Chaos, Solitons & Fractals* 11 (15) (2000) 2479–2485.
[17] S. Natsiavas, Stability and bifurcation analysis for oscillators with motion limiting constraints, *Journal of Sound and Vibration* 141 (1) (1990) 97–102.
[18] S.R. Bishop, D. Xu, The use of control to eliminate subharmonic and chaotic impacting motion of a driven beam, *Journal of Sound and Vibration* 205 (2) (1997) 223–234.
[19] S. Ayal De Jayatilawa, *Fracture of Engineering Brittle Materials*, Applied Science Publishers, London, 1979.
[20] J.F. Knott, *Fundamentals of Fracture Mechanics*, Butterworth, Norwich, 1973.
[21] J.D. Landes (Ed.), Nonlinear fracture mechanics, *Proceedings of the Third International Symposium on Nonlinear Fracture*, Knoxville, 1989.
[22] M. Wiercigroch, S.E. Miklailov, EPSRC Project No. GR/R85556 on Nonlinear Dynamics and Contact Fracture Mechanics in Modelling Vibration Enhanced Drilling, Aberdeen, 2002.
[23] S. Banerjee, C. Grebogi, Border collision bifurcations in two-dimensional piecewise smooth maps, *Physical Review E* 59 (4) (1999) 4052–4061.
[24] W. Cin, E. Ott, H.N. Nusse, C. Grebogi, Grazing bifurcations in impact oscillators, *Physical Review E* 50 (6) (1999) 4427–4444.